The important conclusion from these fitting exercises is that long copper-sulfur intermolecular contacts can lead to significant exchange coupling interactions. Other long copper-sulfur intermolecular contacts that give rise to *large* exchange coupling constants include $[Cu(TCH)Cl_2]Cl_2$ (TCH = $1H^+$-thiocarbonylhydrazidium), which has a long copper-sulfur bond in the Cu_2S_2 unit of 3.310 Å[14] and $J = -12.4$ cm^{-1},[15] $[Cu(dmdtc)_2]_\infty$ (dmdtc = dimethyldithiocarbamate), with the long Cu-S bonding being 3.159 Å[16] and $J = -1.2$ cm^{-1},[17] and a series of dithiaalkane alternating-chain compounds of the general formula $[Cu(dithiaalkane)Cl_2]_\infty$.[18] Also germane to this discussion is the observation of a J value of -8.5 cm^{-1} in $[Ni(DDDT)_2]^-$ (DDDT$^-$ = 5,6-dihydro-1,4-dithiin-2,3-dithiolate), in which the shortest Ni-Ni distance is 8.152 Å,[3] and the recent report of a J value of -23.8 cm^{-1} in the sulfur-bridged iron dimer $\{K_2[Fe(dithiooxalato)_2NO]\}_2$, where the long Fe-S contact in the Fe_2S_2 exchange-coupled unit is 3.823 Å.[4]

Antiferromagnetic exchange coupling interactions are reasonably easily detected, even if they are small, since the observed magnetic moments depart from the spin-only moment toward lower values. If the interactions are ferromagnetic, they are significantly more difficult to detect, easpecially in the presence of zero-field splittings and, for clusters, in the presence of antiferromagnetic intermolecular interactions.

Acknowledgment. This research was supported by the National Science Foundation through Grant No. CHE 88 07498 and by NATO through a fellowship to F.N. The X-ray diffractometer at NC State University was upgraded through Grant No. CHE 83 07022 from the National Science Foundation.

Supplementary Material Available: A figure showing the labeling of the non-hydrogen atoms in the second independent molecule in the unit cell and tables of hydrogen atom coordinates, anisotropic thermal parameters, bond lengths, and bond angles (5 pages); a listing of calculated and observed structure factors (16 pages). Ordering information is given on any current masthead page.

(14) Landredi, A. M.; Tiripicchio, A.; Camellini, M. T. *J. Chem. Soc., Dalton Trans.* **1975**, 2168.
(15) Hatfield, W. E.; Richardson, H. W.; Wasson, J. R. *Inorg. Nucl. Chem. Lett.* **1977**, *13*, 137.
(16) Einstein, F. W. B.; Field, J. S. *Acta Crystallogr., Sect. B* **1974**, *B30*, 2928.
(17) Hatfield, W. E.; Weller, R. R.; Hall, J. W. *Inorg. Chem.* **1980**, *19*, 3825.
(18) Hatfield, W. E.; ter Haar, L. W.; Olmstead, M. M.; Musker, W. K. *Inorg. Chem.* **1986**, *25*, 558.

Contribution from the Department of Chemistry, University of Florence, Florence, Italy, and Departement de Recherche Fondamentale, Centre d'Etudes Nucleaires, Grenoble, France

Ferro- and Antiferromagnetic Coupling between Metal Ions and Pyridine-Substituted Nitronyl Nitroxides

Andrea Caneschi,[1a] Fabrizio Ferraro,[1a] Dante Gatteschi,*[,1a] Paul Rey,*[,1b] and Roberta Sessoli[1a]

Received February 5, 1990

The synthesis and crystal structure of two novel adducts of manganese(II) and nitronyl nitroxide radicals of formula $Mn(hfac)_2(NITpPy)_2$ (I) and $MnCl_2(NITpPy)_4$ (II), where hfac = hexafluoroacetylacetonate and NITpPy = 2-(4-pyridyl)-4,4,5,5-tetramethyl-4,5-dihydro-1*H*-imidazolyl-1-oxyl 3-oxide, are reported. Compound I crystallizes in the monoclinic space group $P2_1/n$ with $a = 14.037$ (2) Å, $b = 6.500$ (7) Å, $c = 22.180$ (5) Å, $\beta = 99.39$ (1)°, and $Z = 2$. Compound II crystallizes in the triclinic space group $P\bar{1}$ with $a = 7.205$ (4) Å, $b = 13.613$ (2) Å, $c = 13.630$ (4) Å, $\alpha = 89.74$ (2)°, $\beta = 78.69$ (4)°, $\gamma = 86.88$ (4)°, and $Z = 1$. In both cases the complex is mononuclear with the manganese ion octahedrally coordinated and bound to the nitronyl nitroxide radicals through the nitrogen atom of the pyridine ring. The magnetic susceptibility of both compounds suggests that the manganese ion and the radicals are ferromagnetically coupled with a coupling constant of about 1 cm^{-1}. The nickel(II) analogues, $Ni(hfac)_2(NITpPy)_2$ (III) and $NiCl_2(NITpPy)_4$ (IV), were also synthesized, and IV was found to be isomorphous with II. The magnetic behavior of the nickel derivatives suggests that the metal ion is antiferromagnetically coupled to the radical through the pyridine ring with a coupling constant of about 10 cm^{-1}. The mechanism of exchange was analyzed in terms of orbital pathways involving the π^* molecular orbital of the NITpPy radical containing the unpaired electron, the pyridine nitrogen lone pair, and the metal orbitals.

Introduction

We are currently attempting to synthesize molecular based ferromagnets[2-5] by using metal ions directly bound to stable organic radicals as building blocks.[6] The radicals we have used so far are the *o*-semiquinones[7,8] and the nitronyl nitroxides,[6] NITR (NITR = 2-R-4,4,5,5-tetramethyl-4,5-dihydro-1*H*-imidazolyl-1-oxyl 3-oxide), whose general formula is sketched as follows:

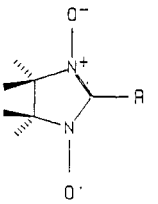

As far as the elementary interactions are concerned, the conditions under which either ferro- or antiferromagnetic coupling is established between the metal ions and the radicals are now

(1) (a) University of Florence. (b) Centre d'Etudes Nucleaires.
(2) Kahn, O. *Angew. Chem., Int. Ed. Engl.* **1985**, *24*, 834.
(3) Miller, J. S.; Epstein, A. J.; Reiff, W. R. *Acc. Chem. Res.* **1988**, *21*, 114.
(4) Korshak, Yu.; Medvedeva, T. V.; Ovchinnikov, A. A.; Spector, V. N. *Nature* **1987**, *326*, 370.
(5) Sugawara, T.; Bandow, S.; Kimura, K.; Iwamura, H.; Itoh, K. *J. Am. Chem. Soc.* **1986**, *108*, 368.
(6) Caneschi, A.; Gatteschi, D.; Sessoli, R.; Rey, P. *Acc. Chem. Res.* **1989**, *22*, 392.
(7) Benelli, C.; Dei, A.; Gatteschi, D.; Pardi, L. *Inorg. Chem.* **1988**, *27*, 2831.
(8) Benelli, C.; Dei, A.; Gatteschi, D.; Pardi, L. *Inorg. Chem.* **1989**, *28*, 1476.

0020-1669/90/1329-4217$02.50/0

clear. In particular we have found that strong ferromagnetic coupling between metal ion and *o*-semiquinones is observed whenever the magnetic orbitals on the metals are σ in nature in a pseudooctahedral coordination, because they are then orthogonal to the π^* orbital of the radical, which contains the unpaired electron.[7] With the nitronyl nitroxides binding through their oxygen atoms the metal–radical interactions are of the same type but weaker: even if ferromagnetic coupling can be obtained also in this case whenever the metal and ligand magnetic orbitals are orthogonal to each other,[9,10] the extent of the interaction is much smaller for these complexes. For instance we observe a ferromagnetic $|J|$ value, defined by the spin Hamiltonian $H = JS_1S_2$, larger than 400 cm^{-1} for a nickel(II) semiquinone complex,[7] while the largest value observed for a copper(II) nitronyl nitroxide complex has been 70 cm^{-1}.[9]

We observed a ferromagnetic coupling also in gadolinium(III) complexes with nitronyl nitroxides, with J of the order of 1 cm^{-1}.[11] In that case we postulated that the main pathway responsible of the observed weak ferromagnetic coupling is the nonzero overlap of the π^* orbital with an empty s orbital of gadolinium: the transfer of a fraction of unpaired electron density in this empty orbital keeps the spins of the electrons in the f orbitals parallel with respect to each other, thus justifying the observed ferromagnetic coupling. Confirmation of the involvement of the empty s orbitals in the exchange pathways comes from the relatively large superexchange interaction between two nitronyl nitroxides bridged by a yttrium(III) ion.[12]

With the nitronyl nitroxides we succeeded indeed in synthesizing molecular based materials exhibiting spontaneous magnetization at low temperature.[13-16] However, the highest T_c values we obtained are still in the range of 20 K, essentially because we could connect metal ions and radicals in one-dimensional but not three-dimensional structures. The intrachain interactions are relatively strong, but the interchain ones are at least 3 orders of magnitude weaker, thus demanding low temperatures to achieve magnetic order. In order to increase the interactions between these low-dimensional magnetic materials we decided to use NITR radicals in which the R group has an additional donor atom in the hope to provide more exchange pathways, which eventually increase T_c.

With these considerations in mind we addressed ourselves to NITpPy (NITpPy = 2-(4-pyridyl)-4,4,5,5-tetramethyl-4,5-dihydro-1*H*-imidazolyl-1-oxyl 3-oxide), which, on the basis of solution studies, was shown to bind to metal ions through the pyridine nitrogen atom and nevertheless was reported to yield very strong antiferromagnetic coupling with copper(II),[17,18] oxovanadium(IV),[18,20] and manganese(II).[19] We previously reported a crystalline compound of formula $CuCl_2(NITpPy)_2$, whose X-ray analysis confirmed that the nitronyl nitroxide binds to copper through the pyridine nitrogen.[21] The coupling between copper and radical was found to be antiferromagnetic, with $J \cong 20$ cm^{-1}. This was an important result, because it showed how the metal and radical can feel each other even through a pyridine ring, thus opening the possibility to active long-range coupling in the solid state, even if the observed coupling is much smaller than that reported in solution studies.[17-20]

In order to determine how the nature of the metal influences the coupling of the NITpPy radical we decided to study manganese(II) and nickel(II) complexes. We wish to report here the X-ray crystal structure of two compounds of formula $Mn(hfac)_2(NITpPy)_2$ (I) and $MnCl_2(NITpPy)_4$ (II), in which the manganese(II) ions are bound to two and four NITpPy radicals, respectively. The analysis of the magnetic properties of these compounds, and of those of the analogous nickel derivatives, $Ni(hfac)_2(NITpPy)_2$ (III) and $NiCl_2(NITpPy)_4$ (IV), showed that the metal–radical coupling is ferromagnetic for manganese and antiferromagnetic for nickel, and we want to justify this behavior on the basis of orbital pathways.

Table I. Crystallographic and Experimental Parameters for $Mn(hfac)_2(NITpPy)_2$ (I) and $MnCl_2(NITpPy)_4$ (II)

	I	II
formula	$MnC_{34}F_{12}H_{34}N_6O_8$	$MnC_{48}Cl_2H_{64}N_{12}O_8$
fw	937.6	1062.9
cryst syst	monoclinic	triclinic
space group	$P2/n$	$P\bar{1}$
a, Å	14.037 (2)	7.205 (4)
b, Å	6.500 (7)	13.613 (2)
c, Å	22.180 (5)	13.630 (4)
α, deg		89.74 (2)
β, deg	99.39 (1)	78.69 (4)
γ, deg		86.88 (4)
V, Å^3	1996.7	1308.9
Z	2	1
ρ_{calcd}, g/cm^3	1.559	1.348
μ, cm^{-1}	3.89	3.69
T, °C	20	
radiation (λ, Å)	Mo Kα (0.7107)	
R	6.44	5.43
R_w	6.81	5.35

Experimental Section

Synthesis of the Complexes. $Mn(hfac)_2(NITpPy)_2$. $Mn(hfac)_2 \cdot 2H_2O$ was prepared as previously described.[22] NITpPy was prepared according to the literature method.[23] A 0.5-mmol amount of $Mn(hfac)_2 \cdot 2H_2O$ was dissolved in 15 mL of absolute ethanol, and then 1 mmol of the NITpPy radical was added. The green solution was allowed to stay at room temperature for 4 days, and then light green crystals were collected that analyzed well for $Mn(hfac)_2(NITpPy)_2$. Anal. Calcd for $C_{34}F_{12}H_{34}MnN_6O_8$: C, 43.53; H, 3.63; N, 8.96. Found: C, 43.43; H, 3.60; N, 8.89.

$MnCl_2(NITpPy)_4$. Solutions containing 1 mmol of $MnCl_2 \cdot 4H_2O$ (Aldrich Co.) and 2 mmol of NITpPy in absolute ethanol were allowed to react at 20 °C by slow diffusion. Little green crystals were collected after 3 months, and they analyzed well for $MnCl_2(NITpPy)_4$. Anal. Calcd for $C_{48}Cl_2H_{64}MnN_{12}O_8$: C, 54.24; H, 6.03; N, 15.81. Found: C, 54.19; H, 6.06; N, 15.75.

$Ni(hfac)_2(NITpPy)_2$. $Ni(hfac)_2 \cdot 2H_2O$ was prepared as previously described.[15] A 0.5-mmol amount of $Ni(hfac)_2 \cdot H_2O$ were dissolved in 20 mL of absolute ethanol, and then a solution of 30 mL of absolute ethanol containing 1 mmol of NITpPy radical was added. Immediately a light green microcrystalline precipitate appeared. It was filtered out, and it analyzed well for $Ni(hfac)_2(NITpPy)_2$. Anal. Calcd for $C_{34}F_{12}H_{34}N_6NiO_8$: C, 43.36; H, 3.61; N, 8.93. Found: C, 43.47; H, 3.72; N, 8.90.

$NiCl_2(NITpPy)_4$. A hot ethanol solution containing 0.5 mmol of $NiCl_2 \cdot 6H_2O$ (Aldrich Co). was mixed with a warm solution containing 1 mmol of NITpPy radical. Immediately a light green powder precipitated that analyzed well for $NiCl_2(NITpPy)_4$. Anal. Calcd for $C_{48}Cl_2H_{64}N_{12}NiO_8$: C, 54.03; H, 6.00; N, 15.76. Found: C, 53.86; H, 5.91; N, 15.60.

X-ray Analysis and Structure Determination. Well-shaped green crystals of I and II, obtained as described above, were suitable for X-ray analysis. The data for both compounds were collected at room temperature with an Enraf-Nonius CAD4 four-circle diffractometer using

(9) Caneschi, A.; Gatteschi, D.; Grand, A.; Laugier, J.; Pardi, L.; Rey, P. *Inorg. Chem.* **1988**, *27*, 1031.
(10) Caneschi, A.; Gatteschi, D.; Laugier, J.; Rey, P. *J. Am. Chem. Soc.* **1987**, *109*, 2191.
(11) Benelli, C.; Caneschi, A.; Gatteschi, D.; Pardi, L.; Rey, P.; Shum, D. P.; Carlin, R. L. *Inorg. Chem.* **1989**, *28*, 272.
(12) Benelli, C.; Caneschi, A.; Gatteschi, D.; Pardi, L.; Rey, P. *Inorg. Chem.* **1989**, *28*, 3230.
(13) Caneschi, A.; Gatteschi, D.; Renard, J.-P.; Rey, P.; Sessoli, R. *Inorg. Chem.* **1989**, *28*, 1976.
(14) Caneschi, A.; Gatteschi, D.; Renard, J.-P.; Rey, P.; Sessoli, R. *Inorg. Chem.* **1989**, *28*, 3314.
(15) Caneschi, A.; Gatteschi, D.; Renard, J.-P.; Rey, P.; Sessoli, R. *Inorg. Chem.* **1989**, *28*, 2940.
(16) Caneschi, A.; Gatteschi, D.; Renard, J.-P.; Rey, P.; Sessoli, R. *J. Am. Chem. Soc.* **1989**, *111*, 785.
(17) Richardson, P. F.; Kreilick, R. W. *J. Am. Chem. Soc.* **1977**, *99*, 8183.
(18) Richardson, P. F.; Kreilick, R. W. *J. Magn. Reson.* **1978**, *29*, 285.
(19) Richardson, P. F.; Kreilick, R. W. *J. Phys. Chem.* **1978**, *82*, 1149.
(20) Richardson, P. F.; Kreilick, R. W. *Chem. Phys. Lett.* **1977**, *50*, 333.
(21) Caneschi, A.; Ferraro, F.; Gatteschi, D.; Rey, P.; Sessoli, R. *Inorg. Chem.* **1990**, *29*, 1756.
(22) Cotton, F. A.; Holm, R. H. *J. Am. Chem. Soc.* **1960**, *82*, 2979.
(23) Ullman, E. F.; Call, L.; Osiecki, J. H. *J. Org. Chem.* **1970**, *35*, 3623. Davis, M. S.; Morokuma, K.; Kreilick, R. W. *J. Am. Chem. Soc.* **1972**, *94*, 5588.

Table II. Atomic Coordinates ($\times 10^4$) and Isotropic Thermal Factors ($Å^2 \times 10^3$) for $Mn(hfac)_2(NITpPy)_2$ (I)[a]

	x/a	y/b	z/c	U_{iso}
Mn	0	0	0	34
O1	-63 (3)	-2106 (7)	741 (2)	36
O2	1130 (3)	1455 (7)	645 (2)	41
O3	-3405 (4)	3687 (9)	1918 (3)	66
O4	-3698 (4)	7935 (9)	225 (3)	60
N1	-3673 (4)	5081 (10)	1522 (3)	42
N2	-3837 (4)	7116 (10)	720 (3)	40
N3	-1173 (4)	1958 (9)	327 (3)	37
C1	395 (5)	-2025 (11)	1267 (3)	33
C2	1118 (5)	-668 (12)	1514 (4)	47
C3	1426 (5)	971 (11)	1180 (3)	37
C4	40 (7)	-3581 (13)	1696 (4)	50
C5	2264 (7)	2225 (17)	1507 (5)	67
C6	-2599 (5)	4304 (11)	754 (3)	36
C7	-2335 (6)	2337 (12)	1001 (4)	53
C8	-1641 (6)	1269 (11)	759 (4)	51
C8	-1641 (6)	1269 (11)	759 (4)	51
C9	-1428 (5)	3867 (12)	99 (3)	44
C10	-2134 (5)	5016 (13)	302 (3)	39
C11	-3349 (5)	5468 (11)	998 (3)	35
C12	-4324 (5)	6796 (12)	1675 (3)	44
C13	-4663 (5)	7659 (11)	1034 (4)	42
C14	-5106 (7)	5938 (15)	2001 (5)	77
C15	-3640 (7)	8247 (14)	2099 (4)	68
C16	-5541 (6)	6594 (15)	684 (4)	68
C17	-4829 (6)	10033 (13)	1007 (4)	60
F1	28 (4)	-5493 (7)	1464 (2)	75
F2	566 (4)	-3682 (8)	2245 (2)	80
F3	-852 (4)	-3176 (9)	1769 (3)	81
F4	2269 (5)	2459 (12)	2090 (3)	128
F5	2246 (6)	4137 (12)	1306 (4)	150
F6	3057 (5)	1551 (17)	1452 (6)	229

[a] Standard deviations in the last significant digit are in parentheses.

graphite-monochromated Mo Kα radiation. Data were corrected for Lorentz and polarization effects but not for absorption. More details are given in Table SI (supplementary material), of which Table I is a condensed form.

Compound I crystallizes in the monoclinic system, and the space group $P2_1/n$ was univocally determined by the systematic extinctions. The Patterson map revealed the position of the manganese atom, which lies in a special position. The other non-hydrogen atoms were found by successive Fourier syntheses using the SHELX76 package.[24] Anistropic thermal factors were introduced for the metal atom, the oxygen atom, the fluorine atom, and eight carbon atoms. A pronounced anisotropic thermal motion was found in the CF_3 groups, which show however a reasonable geometry. The presence of thermal motion and the fact that the manganese atom contributes only to half of the structure factors sensibly affect the precision of the structure. In fact, the final refinement, including the contribution of hydrogen atoms in fixed and idealized positions, converged to $R = 0.064$. The highest peak in the last Fourier difference synthesis was about 0.5 e/Å^3 and was located close to the metal atom.

Compound II crystallizes in the tricylinic space group $P\bar{1}$. The structure solution was performed as described for I. All atoms, including the hydrogens, were found by successive Fourier syntheses. The final refinement with anisotropic thermal factors for all non-hydrogen atoms converged to $R = 0.054$. The highest peak in the last Fourier difference synthesis was again located close to the metal atom and corresponds to 0.5 e/Å^3.

Final atomic coordinates are reported in Tables II and III for compounds I and II, respectively.

Powder diffractograms were recorded with a Philips generator equipped with Cu Kα radiation and a Model PW1710 detection chain.

Magnetic Measurements and EPR Spectra. The magnetic susceptibility of I and II in the temperature range 5–300 K was measured in a magnetic field of 0.5 T by using an SHE superconducting SQUID magnetometer, while the susceptibility of III and IV was measured with a Faraday Aztec DSM5 susceptometer equipped with an Oxford Instruments CF1300S continuous-flow cryostat in a magneti field of 1.35 T. Data were corrected for the magnetization of the sample holder and for diamagnetic contributions, which were estimated from Pascal's constants.

EPR spectra of polycrystalline powders were recorded with a Varian E-9 spectrometer equipped with standard X-band facilities. Low-temperature spectra were recorded by using an Oxford Instruments ESR9 liquid-helium continuous-flow cryostat.

Calculations. The extended Huckel calculations of the molecular orbitals of the NITpPy radical were performed on an IBM 4361/3 computer. The Slater exponents and VSIP parameters were taken from the literature.[25]

Table III. Positional Parameters ($\times 10^4$) and Isotropic Thermal Factors ($Å^2 \times 10^3$) for $MnCl_2(NITpPy)_4$ (II)[a]

	x/a	y/b	z/c	U_{iso}
Mn	0	0	0	22
Cl1	3087 (2)	461 (1)	-953 (1)	35
O1	123 (5)	4770 (3)	-2237 (3)	55
O2	-6190 (5)	4371 (3)	-907 (4)	64
O3	4669 (5)	1859 (3)	3965 (3)	46
O4	-1478 (5)	1106 (3)	5278 (3)	56
N1	-1256 (5)	1583 (3)	-276 (3)	30
N2	-1694 (6)	4911 (3)	-1997 (3)	37
N3	-4682 (6)	4705 (3)	-1429 (4)	41
N4	629 (5)	689 (3)	1452 (3)	30
N5	3154 (5)	1705 (3)	4590 (3)	29
N6	178 (5)	1428 (3)	5193 (3)	35
C1	-123 (7)	2345 (4)	-402 (4)	33
C2	-595 (7)	3239 (4)	-748 (4)	34
C3	-2381 (7)	3404 (4)	-1007 (4)	32
C4	-3595 (7)	2631 (4)	-848 (4)	32
C5	-2994 (7)	1755 (4)	-492 (4)	32
C6	-2895 (7)	4313 (4)	-1451 (4)	34
C7	-2640 (7)	5845 (4)	-2269 (4)	37
C8	-4717 (7)	5516 (4)	-2151 (4)	39
C9	-1735 (11)	6141 (6)	-3325 (5)	56
C10	-2417 (11)	6613 (5)	-1501 (6)	54
C11	-5154 (10)	5049 (6)	-3084 (6)	55
C12	-6240 (10)	6315 (6)	-1763 (6)	57
C13	2358 (7)	594 (4)	1697 (4)	30
C14	2707 (7)	815 (4)	2612 (4)	30
C15	1240 (6)	1174 (3)	3359 (3)	27
C16	-560 (6)	1325 (4)	3111 (4)	30
C17	-777 (7)	1074 (4)	2171 (4)	33
C18	1528 (6)	1413 (4)	4344 (3)	28
C19	796 (7)	1933 (4)	6038 (4)	33
C20	2991 (7)	1800 (4)	5697 (3)	32
C21	-4 (10)	1453 (6)	7018 (4)	46
C22	021 (10)	2986 (5)	6021 (5)	51
C23	3797 (8)	835 (5)	6035 (5)	47
C24	4069 (11)	2657 (6)	5935 (6)	58

[a] Standard deviations in the last significant digit are in parentheses.

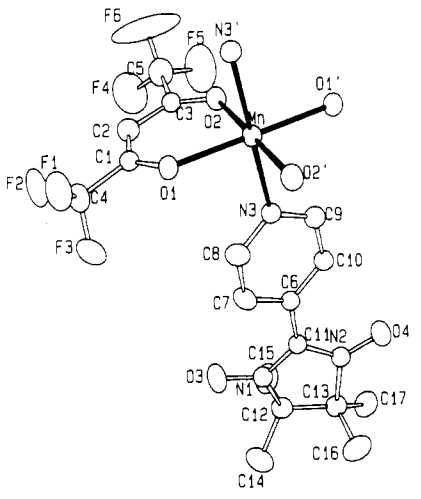

Figure 1. ORTEP view of the asymmetric unit of $Mn(hfac)_2(NITpPy)_2$ at 40% probability.

(24) Sheldrick, G. SHELX76 System of Computing Programs. University of Cambridge, England, 1976. Atomic scattering factors: Cromer, D. T.; Lieberman, D. *J. Chem. Phys.* **1970**, *53*, 1891.

(25) Hay, P. J.; Thibeault, J. C.; Hoffmann, R. *J. Am. Chem. Soc.* **1975**, *97*, 4884.

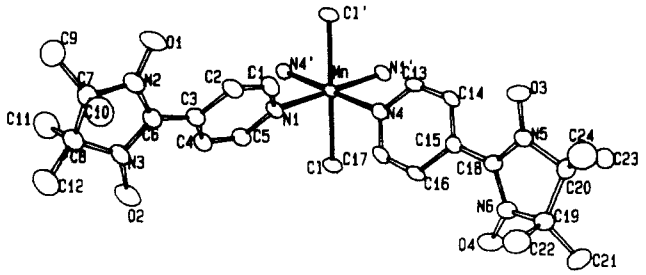

Figure 2. ORTEP view of the asymmetric unit of $MnCl_2(NITpPy)_4$ at 50% probability.

Table IV. Selected Bond Distances (Å) and Angles (deg) for $Mn(hfac)_2(NITpPy)_2$ (I) and $MnCl_2(NITpPY)_4$ (II)[a]

		I	
Mn–O1	2.151 (5)	Mn–O2	2.172 (4)
Mn–N3	2.290 (6)	O3–N1	1.275 (8)
O4–N2	1.264 (9)	N1–C11	1.339 (9)
N2–C11	1.363 (9)		
O1–Mn–N3	89.5 (2)	O2–Mn–N3	92.0 (2)
O1–Mn–O2	83.7 (2)		
		II	
Mn–Cl	2.458 (2)	Mn–N1	2.348 (4)
Mn–N4	2.328 (4)	O1–N2	1.272 (5)
O2–N3	1.281 (6)	O3–N5	1.272 (5)
O2–N3	1.281 (6)	O3–N5	1.272 (5)
O4–N6	1.277 (6)	N2–C6	1.336 (6)
N3–C6	1.361 (6)	N5–C18	1.360 (6)
N6–C18	1.358 (5)		
N1–Mn–N4	84.7 (2)	Cl–Mn–N1	88.9 (1)
Cl–Mn–N4	91.0 (1)		

[a] Standard deviations in the last significant digit are in parentheses.

Results and Discussion

Crystal Structures. In the compound $Mn(hfac)_2(NITpPy)_2$ (I), the manganese ion lies on an inversion center and is coordinated by four oxygen atoms of the β-diketonates and two nitrogen atoms of the pyridine groups of two radicals, as shown in Figure 1. The Mn–N bond is longer than the Mn–O bonds (2.29 vs 2.16 Å), and the coordination geometry is that of an elongated octahedron. The bond distances and angles within the radicals are fairly normal and compare well with those previously reported.[9,10,14,15,21] The five-membered ring of the radical deviates significantly from planarity with C_{12} and C_{13} 0.18 Å above and below the average plane, respectively. The pyridine ring is planar and makes an angle of 16.4° with the plane of the radical defined by the atoms O3, N1, C11, N2, and O4. The molecular units are well separated one from each other, and no contact shorter than 5 Å is present between the N–O groups of radicals belonging to different units.

A similar coordination was found for $MnCl_2(NITpPy)_4$ (II), whose asymmetric unit is reported in Figure 2, where the coordination octahedron is formed by two chlorine atoms and four nitrogen atoms of the pyridine rings of four radicals. Also in this case the metal ion is located on an inversion center and the octahedron is elongated along the Mn–Cl bonds (2.468 vs 2.33 Å). The geometry of the two nonequivalent radicals is substantially similar to that observed in I. The angles between the pyridine ring and the ONCNO planes are 29.01 and 29.63° for the two nonequivalent radicals.

In the case of II, where no shielding due to the steric hindrance of the hexafluoroacetylacetonates is present, the noncoordinated N–O groups are at relatively short distances from those of other molecular units. In particular we found that each radical has two neighbors at about 3.6 Å, which are related by the translation along the *a* axis. Similar contacts were found also between each radical and the centrosymmetric ones translated along the *c* axis and along the (−1,1,0) direction.

Selected bond lengths and angles for I and II are given in Table IV, while a complete listing is available as supplementary material.

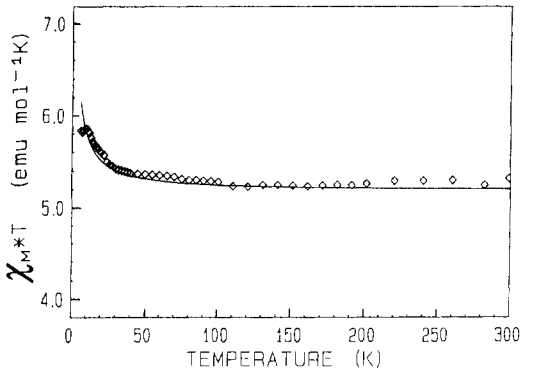

Figure 3. Temperature dependence of the magnetic susceptibility of $Mn(hfac)_2(NITpPy)_2$ (I) in the form $\chi_m T$ vs T. The solid line represents the calculated values with the best fit parameters (see text).

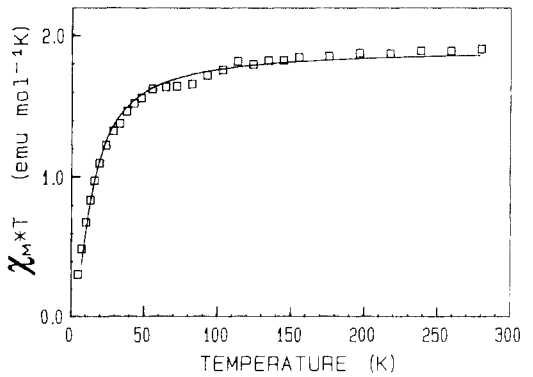

Figure 4. Temperature dependence of the magnetic susceptibility of $Ni(hfac)_2(NItpPy)_2$ (III) in the form $\chi_m T$ vs T. The solid line represents the calculated values with the best fit parameters (see text).

X-ray powder diffractograms have shown that II and IV are isomorphous, while no analogies are found between I and III. A listing of the more intense peaks and relative 2θ angles of II and IV are given as supplementary material. The isomorphism between II and IV suggests that the nickel compound is isostructural to the manganese one.

Although no direct structural information is available for compound III, the elemental analysis together with the magnetic properties suggests that the nickel ion is octahedrally coordinated by two hexafluoroacetylacetonates and two pyridines of the NITpPy radicals as found in the manganese analogues.

Magnetic Measurements. The $\chi_m T$ vs T plot of I is shown in Figure 3. The room-temperature value is 5.24 emu K mol^{-1} (μ_{eff} = 6.47 μ_B), a little higher than the value expected for one $S = {}^5/_2$ and two $S = {}^1/_2$ uncorrelated spins (5.125 emu mol^{-1} K), and increases slowly on lowering the temperature, thus showing the presence of a weak ferromagnetic interaction. A round maximum of 5.86 emu K mol^{-1} (μ_{eff} = 6.85 μ_B) is reached at 10 K.

The magnetic susceptibility of $Ni(hfac)_2(NITpPy)_2$ (III) is shown in Figure 4. Contrary to the manganese analogue, in this case χT decreases on decreasing temperature, from a room-temperature value of 1.9 emu K mol^{-1} (μ_{eff} = 3.90 μ_B) to 0.49 emu K mol^{-1} (μ_{eff} = 1.97 μ_B) at 7.4 K. These values should be compared to the spin-only value expected for noncoupled spins of 1.7 emu K mol^{-1} (μ_{eff} = 3.7 μ_B).

The experimental data were reproduced by using a standard procedure for three coupled spins with the symmetry of an isosceles triangle.[26] The saturation effects were introduced in the calculation by use of Brillouin functions; however, they do not suffice for reproducing the round maximum in the $\chi_m T$ vs T plot of I. The value of the coupling constant between the spin of manganese and those of the radicals that best reproduces the experimental data is J = −1.06 (10) cm^{-1}, where the negative sign indicates ferromagnetic interactions, with $r = 2.14 \times 10^{-4}$.[27] Using the

(26) Carlin, R. L. *Magnetochemistry*; Springer-Verlag: Berlin, 1986.

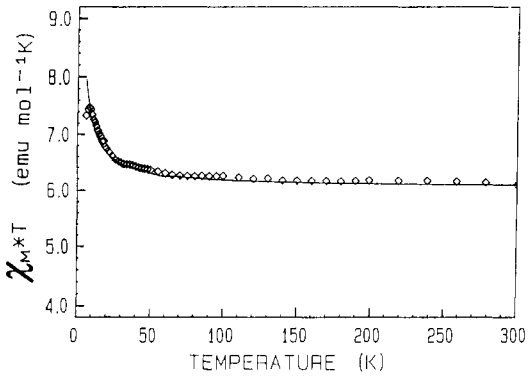

Figure 5. Temperature dependence of the magnetic susceptibility of $MnCl_2(NITpPy)_4$ (II) in the form $\chi_m T$ vs T. The solid line represents the calculated values with the best fit parameters (see text).

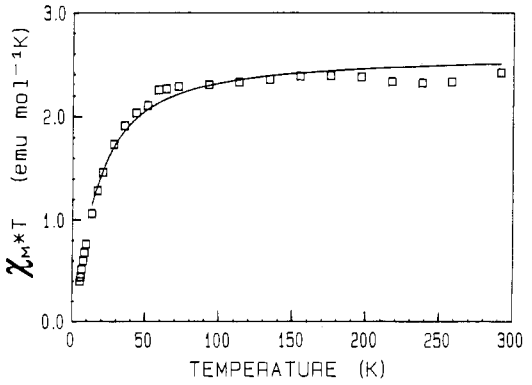

Figure 6. Temperature dependence of the magnetic susceptibility of $NiCl_2(NITpPy)_4$ (II) in the form $\chi_m T$ vs T. The solid line represents the calculated values with the best fit parameters (see text).

same model for III, we obtained a satisfactory fitting with J = 10.0 (5) cm^{-1}; g_{ni} = 2.16 (2), and $r = 6.0 \times 10^{-4}$. These values compare well with those of the compound IV discussed below and confirm our hypothesis that the manganese and nickel derivatives have similar octahedral coordination. The analysis of the magnetic data suggests a $S = {}^7/_2$ ground state for I and $S = 0$ for III.

The temperature behavior of the magnetic susceptibility of II is qualitatively similar to that of I, as can be seen in Figure 5, and gives evidence that also in this compound a weak ferromagnetic interaction is active. The room-temperature value of the product $\chi_m T$ is 6.10 emu mol^{-1} K (μ_{eff} = 6.98 μ_B), a little higher than the uncorrelated spin value (5.875 emu mol^{-1} K), and increases steadily on decreasing the temperature. A maximum in the $\chi_m T$ curve, 7.48 emu K mol^{-1}, is reached at 8 K, and a rapid decrease is observed below this temperature.

The corresponding plot for $NiCl_2(NITpPy)_4$ (IV) has an opposite behavior, as shown in Figure 6, with χT decreasing from the room-temperature value of 2.5 emu K mol^{-1} (μ_{eff} = 4.47 μ_B) to 1.1 emu K mol^{-1} at 13 K, indicating an antiferromagnetic coupling between the nickel and radical spins. Below this temperature a faster decrease of χT is observed, which corresponds to a round maximum in the susceptibility.

The magnetic susceptibility of II and IV was calculated with the highly symmetric scheme of interactions shown as follows:

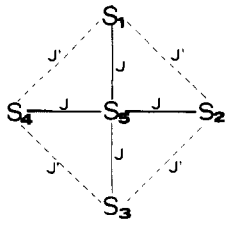

Spin clusters of this kind are still relatively rare and deserve some attention.

The energy levels were obtained by coupling the spins S_1 and S_2 to give S_{12}, S_3 and S_4 to give S_{34}, S_{12} and S_{34} to give S^*, and S^* with S_5 to give S. The total spin states are grouped as follows: for II one state with $S = {}^9/_2$, four with $S = {}^7/_2$, six with $S = {}^5/_2$, four with $S = {}^3/_2$, and one with $S = {}^1/_2$; for IV one state with $S = 3$, four with $S = 2$, six with $S = 1$, and three with $S = 0$. The energies associated with these states are easily expressed in the simplifying assumption that the relevant spin Hamiltonian can be written as

$$H = J'(S_1S_2 + S_2S_3 + S_3S_4 + S_4S_1) + J(S_1 + S_2 + S_3 + S_4)S_5$$

If $S_1 = S_2 = S_3 = S_4 = {}^1/_2$, the energy and g factor of the states defined as $|S_{12}S_{34}S^*S\rangle$ are expressed by[29]

$$E(|S_{12}S_{34}S^*S\rangle) = {}^1/_2J'[S^*(S^* + 1) - S_{12}(S_{12} + 1) - S_{34}(S_{34} + 1)] + {}^1/_2J[S(S + 1) - S^*(S^* + 1) - S_5(S_5 + 1)]$$

$$g = c_a g_a + c_b g_b$$

$$c = [S^*(S^* + 1) - S_5(S_5 + 1)]/[S(S + 1)]$$

$$c_a = (1 + c)/2 \qquad c_b = (1 - c)/2$$

where g_a is the g factor of the peripheral $S = {}^1/_2$ spins and g_b is that of the central spin. When $J' = 0$, the ground state corresponds to the spin distribution with the central spin up and all the peripheral spins down, if J is positive, and with all the spins up, if J is negative. On the other hand when J' is dominant and antiferromagnetic, the ground state becomes the one with peripheral spins completely paired and the central one frustrated, so that the corresponding total spin state has $S = S_5$.

The experimental magnetic data suggest that the ground state for the cluster is $S = {}^9/_2$ for manganese and $S = 1$ for nickel as expected for J ferro- and antiferromagnetic, respectively.

In this treatment we have neglected anisotropic and antisymmetric spin-exchange effects even if the high degeneracy of the total spin states so computed can amplify their effects.[28] The assumption is better suited to the manganese cluster than to the nickel one, but the susceptibility analysis of the experimental data described below suggests that the anisotropy effects are in any case negligible.

The minimization based on a standard least-squares procedure yields a best fit value of the coupling constant J between the metal and the radicals of −0.95 (8) cm^{-1}, with $r = 3.16 \times 10^{-4}$, for II and J = 9.4 (7) cm^{-1}, with $r = 1.5 \times 10^{-3}$, for IV. No significant interaction between the radicals is detected so that J' remains fixed at zero. The rapid decrease of the χT curve below 8 K cannot be accounted for by the saturation effects of the magnetic field but is probably due to antiferromagnetic interactions between different molecular units. Similar considerations apply for IV. We have often observed significant antiferromagnetic interaction when noncoordinated N–O groups of the radicals are at relatively short distance (3.5–4.0 Å) from each other.[21,30,31] In the present case these interactions are not confined in pairs or clusters but form extended chains. No model is available to take into account such a complex network of interactions, and therefore, we do not attempt a quantitative justification of the magnetic behavior at low temperature.

The EPR spectra of polycrystalline powders of I and II consist of a single symmetric broad line centered at $g = 2$. At room temperature the line widths are 286 and 713 G for I and II, respectively. The line widths increase markedly on lowering the temperature down to 4.2 K, but the line shape remains unchanged.

(27) r is defined as $\sum(\chi T_{calc} - \chi T_{oss})^2/\sum(\chi T_{oss})^2$.

(28) Tsukerblat, B. S.; Belinski, M. I.; Fanzil'berg, V. E. *Sov. Chem. Rev.* **1987**, *9*, 339.

(29) Bencini, A.; Gatteschi, D. *Electron Paramagnetic Resonance of Exchange Coupled Systems*; Springer-Verlag: Berlin, Heidelberg, 1990.

(30) Caneschi, A.; Gatteschi, D.; Laugier, J.; Rey, P.; Sessoli, R. *Inorg. Chem.* **1988**, *27*, 1553.

(31) Laugier, J.; Rey, P.; Benelli, C.; Gatteschi, D.; Zanchini, C. *J. Am. Chem. Soc.* **1986**, *108*, 6931.

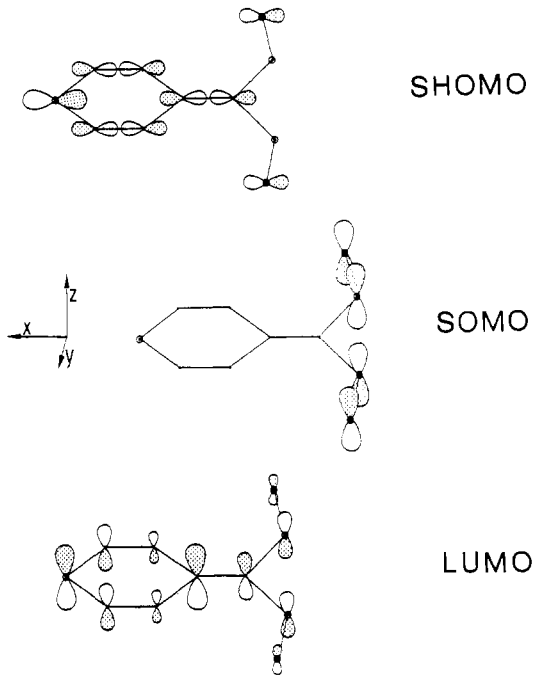

Figure 7. Schematic representation of three molecular orbitals calculated with $\beta = 0°$. The calculated energies are SHOMO $E = -12.20$ eV, SOMO $E = -11.567$ eV, and LUMO $E = -9.46$ eV.

No EPR signal is observed for III and IV.

Mechanism of Exchange. The present results confirm that relatively strong exchange interactions can be transmitted through the pyridine ring of NITR radicals.[17-21] In particular antiferromagnetic coupling is observed for copper(II)[21] and nickel(II) ions, which have magnetic orbitals of σ symmetry relative to the metal–ligand interaction, while ferromagnetic interactions are observed for manganese, which has both σ and π magnetic orbitals.

Long-range exchange interactions were previously observed in solution studies of pyridine-substituted nitroxide complexes, and both ferro- and antiferromagnetic couplings were observed.[32-37] However, the J values are much smaller than those we observe in the present case, probably because in the nitroxides the aromatic rings are connected to the NO group by extensive σ bonds, while in NITpPy the aromatic ring is directly connected to the ONCNO conjugate moiety. On the other hand, our exchange coupling constants, based on data from well-characterized solid derivatives, are much smaller than those previously reported for NITpPy–metal ion interactions.[17-20]

In order to gain insight into the mechanism of exchange, it is useful to have an idea of the MO's of the NITpPy radical. The EH method appears to be very useful for this purpose in order to individuate the ligand magnetic orbitals that can interact with the metal orbitals. We calculate the energy levels for a simplified geometry corresponding to the formula C_5H_5N–$CH_2N_2O_2$, in which the nitronyl nitroxide has two $C(CH_3)_2$ groups substituted by two hydrogen atoms. First we made a calculation in which the angle between the pyridine ring and the ONCNO plane, β, was taken equal to 0°, while in a second calculation β was taken equal to 30°. The significant molecular orbitals obtained in the second calculation are not quantitatively very different from those of the first one; however, when $\beta = 30°$, atomic orbitals of the pyridine ring, in particular the pyridine nitrogen lone pair, also contribute to the SOMO, because the σ and π^* orbitals are no longer orthogonal. The nonorthogonality of the σ and π^* orbitals is preserved in any case if $\beta \neq 90°$. The SOMO is the π^* orbital mainly centered on the NO groups, with the LUMO and SHOMO as shown in Figure 7. In particular the SHOMO has mainly σ character in the aromatic ring, with large contribution of the pyridine nitrogen lone pair. The LUMO has π character in the aromatic ring.

In order to identify possible orbital pathways for exchange interactions, it is useful to look at the symmetry of a metal–radical pair. This has C_{2v} symmetry when α, the angle between the molecular plane of the distorted coordination octahedron and the aromatic ring, is equal to 0° or 90°, and $\beta = 0°$ or 90°, while the symmetry is reduced to C_2 when the above conditions do not obtain. In a reference frame in which x is parallel to the metal–pyridine nitrogen bond the $d_{x^2-y^2}$ and d_{z^2} orbitals have a symmetry and they are not orthogonal to the π^* SOMO orbital, which has also a symmetry. Therefore, the coupling is predicted[37] to be antiferromagnetic for these metal orbitals, and largely independent of α because the overlap between metal and ligand orbitals is essentially of the σ type, via the nitrogen lone pair, which has a small component in the SOMO. The overlap is however small, thus justifying the fact that the antiferromagnetic coupling is much smaller than observed in complexes in which the NITR radicals bind through the oxygen atoms.

The coupling constants for the nickel(II) and copper(II) complexes can be decomposed into the sum of contributions related to different metal orbitals[37,38] in the assumption that spin polarization effects can be neglected as

$$J_{Ni} = \tfrac{1}{2}(J_{x^2-y^2,\pi^*} + J_{z^2,\pi^*}) \qquad J_{Cu} = J_{x^2-y^2,\pi^*}$$

The fact that $J_{Ni} < J_{Cu}$ is in agreement with a smaller value of J_{z^2,π^*} compared to $J_{x^2-y^2,\pi^*}$ due to the smaller overlap of $d_{x^2-y^2}$ with π^*.

For the manganese complexes the coupling constant can be decomposed in the same assumption as for the nickel and copper complexes as

$$J_{Mn} = \tfrac{1}{5}(J_{x^2-y^2,\pi^*} + J_{z^2,\pi^*} + J_{xz,\pi^*} + J_{yz,\pi^*} + J_{xy,\pi^*})$$

Therefore, beyond the components already present for copper and nickel, which are still presumably antiferromagnetic in nature, there are three new exchange pathways that are capable of overcoming the other two antiferromagnetic components. The d_{xy} and d_{xz} orbitals span the b representation of C_2, while d_{yz} is of a symmetry. The last orbital has essentially zero overlap with the ligand SOMO orbital, because the nitrogen lone pair is concentrated around the x axis. Indeed, a weak ferromagnetic interaction between the d_{yz} metal orbital and the SOMO orbital of the NITpPy fragment is possible due to accidental orthogonality. The d_{xy} and d_{xz} orbitals are orthogonal to the ligand SOMO. Since they have a relatively large region of overlap with the ligand SOMO, even if the total overlap is zero, they provide an efficient ferromagnetic exchange pathway.[39-41]

The above considerations, which are based on a MO formalism, can be recast in a superexchange formalism if the pyridine ring is considered as a diamagnetic ligand between two paramagnetic centers. So, if the metal–pyridine interaction is considered to be mainly determined by σ interaction, then the $d_{x^2-y^2}$ and d_{z^2} orbitals can overlap with the σ_{py} orbital, and this in turn, when $\beta \neq 0°$, is not orthogonal to the π^* nitroxide orbital. Therefore, there are two antiferromagnetic exchange pathways, which are determined by σ–π nonorthogonality in these systems. The good efficiency of the mechanism in NITpPy is determined by the fact that the π^* orbital and the pyridine nitrogen lone-pair orbital are relatively close in energy, so making any σ–π nonorthogonality effect rather important.

(32) Eaton, S. S.; More, K. M.; Boymel, P. M.; Sawant, B. M.; Eaton, G. R. *J. Magn. Reson.* **1983**, *52*, 435.
(33) More, K. M.; Eaton, G. R.; Eaton, S. S. *J. Magn. Reson.* **1984**, *59*, 497.
(34) Sawant, B. M.; Shroyer, A. L. W.; Eaton, G. R.; Eaton, S. S. *Inorg. Chem.* **1982**, *21*, 1093.
(35) More, K. M.; Eaton, G. R.; Eaton, S. S.; Hideg, K. *Inorg. Chem.* **1986**, *25*, 3865.
(36) Eaton, S. S.; More, K. M.; Boymel, P. M.; Sawant, B. M.; Eaton, G. R. *J. Magn. Reson.* **1984**, *56*, 183.
(37) Anderson, P. W. *Solid State Phys.* **1963**, *14*, 99.
(38) Eremin, M. V.; Rakitin, Y. V. *Phys. Status Solidi B* **1977**, *80*, 579.
(39) Goodenough, J. B. *Phys. Rev.* **1955**, *100*, 564.
(40) Goodenough, J. B. *Phys. Chem. Solids* **1958**, *6*, 287.
(41) Kanamori, J. *Phys. Chem. Solids* **1958**, *10*, 87.

Conclusions

We have shown that relatively large exchange couplings are observed when metal ions bind to the pyridine nitrogen of NITpPy essentially through a $\sigma-\pi$ nonorthogonality mechanism. Further, it is very important that both ferro- and antiferromagnetic couplings can be observed.

These observations have an important consequence for elaborating strategies to design molecules that can offer multiple exchange pathways, potentially capable of allowing the building of three-dimensional magnetic structures. Indeed the nonzero coupling observed when a metal ion is bound to the pyridine nitrogen gives exciting perspectives if the NO groups can be induced to interact with other paramagnetic centers. This has indeed found to be the case with gadolinium(III) ions.[42]

Acknowledgment. The financial support of the CNR, of the Progetto Finalizzato "Materiali Speciali per Tecnologie Avanzate", and of MURST is gratefully acknowledged. Thanks are due also to the Laboratorio di Chimica Applicata of the Università della Calabria, Calabria, Italy.

Supplementary Material Available: Tables SI-SX, listing crystallographic parameters, anisotropic thermal parameters, hydrogen coordinates, bond lengths, bond angles, and least-squares planes for I and II, and Table SXI, reporting the more intense peaks of the X-ray powder diffractograms of II and IV (15 pages); Tables SXII and SXIII, listing observed and calculated structure factors of I and II, respectively (22 pages). Ordering information is given on any current masthead page.

(42) Benelli, C.; Caneschi, A.; Gatteschi, D.; Pardi, L. Work in progress.

Contribution from the Department of Chemistry, University of Florence, Florence, Italy, and Departement de Recherche Fondamentale, Centre d'Etudes Nucleaires, Grenoble, France

Linear-Chain Gadolinium(III) Nitronyl Nitroxide Complexes with Dominant Next-Nearest-Neighbor Magnetic Interactions

Cristiano Benelli,[†] Andrea Caneschi,[†] Dante Gatteschi,*[,†] Luca Pardi,[†] and Paul Rey[‡]

Received February 5, 1990

$Gd(hfac)_3NITiPr$ (hfac = hexafluoroacetylacetonate; NITiPr = 2-isopropyl-4,4,5,5-tetramethyl-4,5-dihyro-1*H*-imidazolyl-1-oxyl 3-oxide) crystallizes in the monoclinic space group $P2_1/n$ with cell parameters a = 11.916 (1) Å, b = 17.625 (9) Å, c = 18.055 (1) Å, β = 96.98 (1)°, V = 3763.82 Å^3, and Z = 4. The structure refinement converged to R = 0.086. The molecular structure of the complex consists of linear chains made up by gadolinium(III) ions bridged by nitronyl nitroxide radicals. The magnetic properties of this compound and of other structurally strictly related lanthanide nitronyl nitroxide complexes are discussed according to a model in which the next-nearest-neighbor interactions are explicitly taken into account. For appropriate values of the exchange parameters the ground state corresponds to a two-spins-up, two-spins-down configuration, which justifies the low effective magnetic moment observed at low temperature.

Introduction

When a spin is under the influence of two neighboring spins that tend to orient it in two opposing ways, the system is said to be magnetically frustrated. The simplest case in which a situation like this occurs is when three spins on a triangle are antiferromagnetically coupled and the preferred spin orientation in the ground state depends on the relative values of the individual coupling constants. Among the practical realizations of this situation, it is worth mentioning the case of Fe_4S_4 ferredoxin,[1] where the understanding of the nature of the frustrated spin triangular arrangement is central to the interpretation of the magnetic properties of the cluster.[2]

The problem of competing interactions in extended magnetic systems has even more far reaching consequences. Spin glasses are, for instance, known to be systems in which competing interactions lead to a spin-frustrated state, and the models that permit the interpretation of the physics of these systems[3,4] have attracted attention even out of the field of magnetic materials. In fact the statistical mechanics that apply to these systems can be usefully applied to develop models for the mechanisms of action of neural networks.[5]

Furthermore, magnetic solids with competing interactions have provided examples of physical systems with fractal dimensionality.[6-8] Helical and conical as well as other exotic magnetic structures have been predicted, and sometimes observed, when competition is present between different magnetic interactions.[9-12]

For their relative simplicity, one-dimensional systems have provided an objective on which to develop and verify theoretical models regarding physical phenomena ranging from collective excitations to transport phenomena and spin dynamics.[13-18] These systems can in principle give rise to competing interactions when the spins are coupled antiferromagnetically to their next-nearest neighbor (nnn) independent of the sign of the interaction with the nearest neighbors (nn). The preferred spin alignment along the chain, however, depends on the relative intensities of the nn and nnn interactions.

Although in the last few years the magnetic properties of several alternating-spin chains have been reported,[19-24] to our knowledge

[†] University of Florence.
[‡] Centre d'Etudes Nucleaires.

(1) Girerd, J. J.; Papaefthymiou, G. C.; Watson, A. D.; Gamp, E.; Hagen, K. S.; Edelstein, N.; Frankel, R. B.; Holm, R. H. *J. Am. Chem. Soc.* **1984**, *106*, 5941.
(2) Papaefthymiou, G. C.; Girerd, J. J.; Moura, I.; Moura, J. J. G.; Munck, E. *J. Am. Chem. Soc.* **1987**, *109*, 4703.
(3) Sherrington, D.; Kirkpatrick, S. *Phys. Rev. Lett.* **1979**, *35*, 1792.
(4) Sherrington, D.; Kirkpatrick, S. *Phys. Rev. B* **1978**, *17*, 983.
(5) Parisi, G. In *Magnetic Properties of Matter*; Borsa, F., Tognetti, V., Eds.; World Scientific Publishing Co. Pte. Ltd.: Singapore, 1988.
(6) von Boehm, J.; Bak, P. *Phys. Rev. Lett.* **1979**, *42*, 122.
(7) Bak, P.; Fukuyama, H. *Phys. Rev. B* **1980**, *21*, 3287.
(8) Mandelbrot, B. B. *The Fractal Geometry of Nature*; W. H. Freeman: New York, 1982.
(9) Harada, I. *J. Phys. Soc. Jpn.* **1984**, *53*, 1643.
(10) Harada, I.; Mikeska, H. J. *Z. Phys. B: Condens. Matter* **1988**, *72*, 391.
(11) Tonegawa, T.; Harada, I. *J. Phys. Soc. Jpn.* **1987**, *56*, 2153.
(12) Rastelli, E.; Tassi, A.; Reatto, L. *Physica C* **1979**, *97B*, 1.
(13) Berlinsky, A. J. In *Highly Conducting One-Dimensional Solids*; Devreese, J. T., Evrad, R. P., Eds.; Plenum Press: New York, 1979; p 1.
(14) Schweitzer, D.; Keller, H. J. In *Organic and Inorganic Low-Dimensional Crystalline Materials*; Delhaes, P.; Drillon, M., Eds.; Plenum Press: New York, 1987; p 219.
(15) Drumheller, J. E. *Magn. Reson. Rev.* **1982**, *7*, 123.
(16) Kokoszka, G. F. In *Low Dimensional Cooperative Phenomena*; Keller, H. J., Ed.; Plenum Press: New York, 1975; p 171.
(17) Richards, P. M. In *Low Dimensional Cooperative Phenomena*; Keller, H. J., Ed.; Plenum Press: New York, 1975; p 147.
(18) Gatteschi, D.; Sessoli, R. *Magn. Reson. Rev.* **1990**, *15*, 1.

0020-1669/90/1329-4223$02.50/0